Adatom Co-Adsorption with Three-Dimensional Cyclophanes on Ag(111)

Journal:	*The Journal of Physical Chemistry*
Manuscript ID	jp-2017-08953w.R1
Manuscript Type:	Article
Date Submitted by the Author:	12-Oct-2017
Complete List of Authors:	Scheil, Katharina; CAU Kiel, IEAP Lorente, Nicolas; Centro de Fisica de Materiales CFM/MPC (CSIC-UPV/EHU), Bocquet, Marie-Laure; Ecole Normale Superieure de Paris, Pôle de Physicochimie théorique Hess, Pascal; Universitat Basel Departement Chemie Mayor, Marcel; University of Basel, Department of Chemistry Berndt, Richard; CAU Kiel, IEAP

Adatom Co-adsorption with Three-Dimensional Cyclophanes on Ag(111)

Katharina Scheil,[†] Nicolás Lorente,[‡] Marie-Laure Bocquet,[¶] Pascal Christian Hess,[§] Marcel Mayor,[§] and Richard Berndt*[,†]

†*Institut für Experimentelle und Angewandte Physik, Christian-Albrechts-Universität, 24098 Kiel, Germany*

‡*Centro de Física de Materiales CFM/MPC (CSIC-UPV/EHU), Paseo Manuel de Lardizabal 5 and Donostia International Physics Center (DIPC), Paseo Manuel de Lardizabal 4, 20018 Donostia-San Sebastián, Spain*

¶*PASTEUR, Département de chimie, École normale supérieure de Paris, PSL Research University, Sorbonne Universités, UPMC Univ. Paris 06, CNRS, 75005 Paris, France*

§*Department of Chemistry, University of Basel, 4056 Basel, Switzerland*

E-mail: berndt@physik.uni-kiel.de

Abstract

The structure of molecular adlayers is of great interest for surface functionalization. As molecular complexity increases, the subtle interplay of the relevant interactions becomes more difficult to unravel. Here, we present a scanning tunneling microscope (STM) and atomic force microscope (AFM) study along with free-energy calculations using density functional theory on two closely related NDI-cyclophane molecules. These three-dimensional double-decker molecules are designed to attach to the substrate with one subunit while the other functional moiety is exposed to the environment. The molecular arrangements obtained on Ag(111) are rationalized by the inclusion of adatoms from the substrate into the structure. The presence of adatoms is identified by a drastic change in corrugation of the STM images that takes place at moderate bias voltages. Our calculations using density functional theory of the system's free energy yield that two adatoms favorably co-adsorbe with the molecules.

Introduction

The delicate balance among surface-adsorbate interactions leads to chemical properties of increasing complexity as new molecules on solid surfaces are explored.[1–3] An important aspect of surface functionalization is the effect of the adsorbed molecules on the surface structure of the substrate. Surprisingly profound modifications of the substrate may occur. For example, Cu-phthalocyanine induces facetting of Ag(110) surfaces.[4] The rather inert C_{60} fullerene can drastically affect the surfaces of coinage metals, which themselves are not very reactive. On Au(110), Ag(100), Au(111) and Cu(111), C_{60} removes substrate atoms and thus increases its coordination with metallic atoms.[5–8] Adsorbed molecules can bind to metallic atoms thus creating complexes. For example, thiols have been shown to be able to bind Au adatoms at gold substrates.[9,10] Another example are the metal organic networks induced by surface adatoms.[11–19] Such effects are not limited to molecules with reactive end groups such as thiols. For example, ethylidyne (C_2H_3) is capable of producing a significant reconstruction

of the Ru (0001) substrate,[20] insulin alters the flat landscape of gold terraces,[21] which also does pentacene.[22]

The above examples highlight the important role of metal adatoms in the creation of adsorbed molecular networks. These adatoms are naturally present on the surface and minimize the system's free energy by coordinating with the molecules in a hierarchy of structures. Unfortunately, it can be very difficult to actually detect the presence of the adatoms themselves. Careful analysis of the structures is usually the only way to conclude on the presence of molecular-adatom interactions. Recent experiments[15] showed that the scanning tunneling microscope (STM) can help to reveal the presence of metallic adatoms. In Ref. 15, an adatom-related electronic state appeared in STM images recorded at elevated bias voltages. However, large biases are often not suitable when working with molecular structures because of the many undesirable processes that can be induced. Here, we show that changes of contrasts at a moderate bias can actually be the sign of the presence of adatoms.

We designed two similar molecules with a double-decker structure. The lower deck is the same in both molecules, and contains a naphthalene diimide (NDI) phane that generally adsorbs on noble-metal surface via dispersion interactions, and an upper deck, with either a stilbene or an azobenzene moiety. The two subunits are linked via alkyl sulfide groups, creating a three-dimensional building block. Due to this structure, the upper deck experiences little interaction with the surface. This type of molecule thus limits the interaction with the substrate to one of its subunits and is expected to preserve the functional properties of the other subunit. Di-alkyl sulfides only physisorb on Au while thiols chemisorb[23] and consequently the sulfide functions are not expected to cause the main molecule-substrate interaction. The molecules were adsorbed on a Ag(111) surface and a striking bias-dependent change of STM images was observed. By performing density functional theory (DFT) calculations and evaluating the adatom-induced changes of Gibbs free energy, we concluded that two Ag adatoms are co-adsorbed between adjacent double decker molecule. These adatoms

are responsible for the unusual contrast changes.

Methods

Both NDI-cyclophanes have been obtained by a high-dillution macrocyclization conditions as displayed in Scheme 1. The precursor bis-*N*,*N*-(2-(methyldisulfanyl)ethyl)naphthalenediimide **1** was obtained by condensing naphthalenetetracarboxylic dianhydride with a fivefold excess of 2-(methyldisulfanyl)ethan-1-amine, which was synthesized according to a reported procedure.[24] Reducing the disulfides of **1** with tributylphosphine in a methanol/THF mixture provided the bis-*N*,*N*-(2-mercaptoethyl)naphthalenediimide **2**, which was used as crude compound without separation from the tributylphosphine oxide. The stilbene and the azobenzene subunits functionalized with terminal benzylic bromides **3**[25] and **4**[26] have both been reported. For the high dilution cyclization reaction, a 500 μmolar solution of **2** and **3** in 1,3-dimethyl-2-imidazolidinone (DMI) was treated with an excess of potassium carbonate (K_2CO_3) and heated to 60°C for 17 hours. The desired NDI-stilbenophane was isolated by column chromatography (CC) and subsequent gel permeation chromatography (GPC) as orange solid in 9 % yield. Applying a similar strategy, a 332 μmolar solution of **2** and **3** in *N*,*N*-dimethyl-formamide (DMF) was prepared, treated with an excess of K_2CO_3 and heated to 75°C for 16 hours. Again isolation by CC and GPC provided the NDI-azobenzenophane as yellow solid in 17 %. Both cyclophanes were fully characterized by ^{1}H- and ^{13}C-NMR spectroscopy, high resolution mass spectrometry, Infrared and UV/Vis spectrometry and melting points.

The experiments were carried out with a combined scanning tunneling microscope (STM) and atomic force microscope (AFM) operated in ultra-high vacuum at $\approx$ 5 K. Ag(111) surfaces were cleaned by alternating cycles of Ar^+ ion bombardment and annealing. Both types of NDI-cyclophane were degassed and subsequently sublimated at $\approx$ 200°C in ultra-high vacuum from a Ta crucible onto the Ag(111) substrate, which was kept at ambient

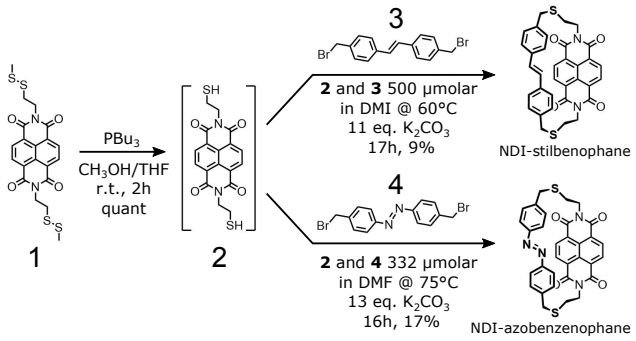

Scheme 1: Syntheses of the two target structures NDI-stilbenophaneand NDI-azobenzenophane.

temperature. Sub-monolayer coverages of ≈ 10 % were typically used. Tips were etched from W wire and prepared in-situ by repeatedly indenting them into the clean areas of the substrate. To measure dI/dV spectra with a lock-in amplifier a sinusoidal modulation of $5 - 10$ $\mathrm{mV_{rms}}$ at 4 kHz was added to the sample voltage.

Ab-initio calculations have been performed in the framework of density functional theory as implemented in the VASP code.[27] We have used the PBE form of the generalized gradient approximation for the exchange and correlation functional.[28] Dispersion interactions have been treated using the method by Tkachenko and Scheffler.[29] The atomic position of the two topmost layers, the adatoms, and the molecules were relaxed until forces were smaller than 0.02 eV/Å. The STM images were simulated using isocontours of the electronic local density of states.[30,31]

Results

Figures 1a and b show schemes of the molecules synthesized for this work, NDI-stilbenophane ((*E*)-1((2,7)-benzo[*lmn*][3,8]phenanthroline-1,3,6,8-(2*H*,7*H*)-tetraona)-6((4,4')-1,2-diphenylethena)-4,8-dithiadecanodane) and NDI-azobenzenophane ((*E*)-1((2,7)-benzo[*lmn*][3,8]phenanthroline1,3,6,8-(2*H*,7*H*)-tetraona)-6((4,4')-1,2-diphenyldiazena)-4,8-dithiadecanodane).[32] Their syntheses are detailed in the *Methods* section. Densely packed islands of these molecules were prepared by sublimation onto Ag(111) surfaces at ambient temperature.

STM data recorded at low temperature (5 K) reveal NDI-stilbenophane and NDI-azobenzenophane islands with similar electronic and geometric properties on the Ag(111) surface. The molecules arrange in a nearly rectangular ($86° \pm 5°$) unit cell, the long axis of which is aligned along a compact direction of the Ag(111) substrate as can be seen in constant-current STM images in Figures 1c,d. The measured unit cell dimensions of (1.8 ± 0.2) nm and (1.0 ± 0.2) nm are compatible with a commensurate $(6 \times 2\sqrt{3})R30°$ molecular lattice on the Ag (111) substrate.

STM topographs recorded at sample voltage V exceeding ≈ 0.6 V exhibit rows of oval protrusions (Figures 1c,d). At first glance, these predominant features seem to correspond to the bulky NDI-stilbenophane and NDI-azobenzenophane molecules. However, the appearance of the islands in topographs critically depends on V. For V below ≈ 0.4 V the topographs reveal features of submolecular dimensions (Figures 1e,f). Cross-sectional profiles of the NDI-stilbenophane data show that the apparent height maxima at low bias fall onto minima at high bias (Figure 1g). The same effect occurs for NDI-azobenzenophane (not shown). Moreover, a drastic change in apparent height by approximately 0.2 nm occurs as the bias is increased from 0.5 to 1.5 V. Figure 1h shows this effect in more detail. The retraction Δz of the tip was measured as a function of V in constant-current mode. The abrupt rise of Δz signals that an additional state is accessible for tunneling as V increases beyond ≈ 0.6 V. Below that voltage, the molecules contribute little to the tunneling current despite their significant dimensions.

Discussion

Changes of intra-layer corrugation with bias have been reported in different situations.[33,34] For single molecules, a corrugation change with bias was reported that disappeared when molecules dimerized.[33] This is clearly not the case here, where the corrugation change happens for the high-coverage case. Another case was due to picking-up oxygen atoms by the

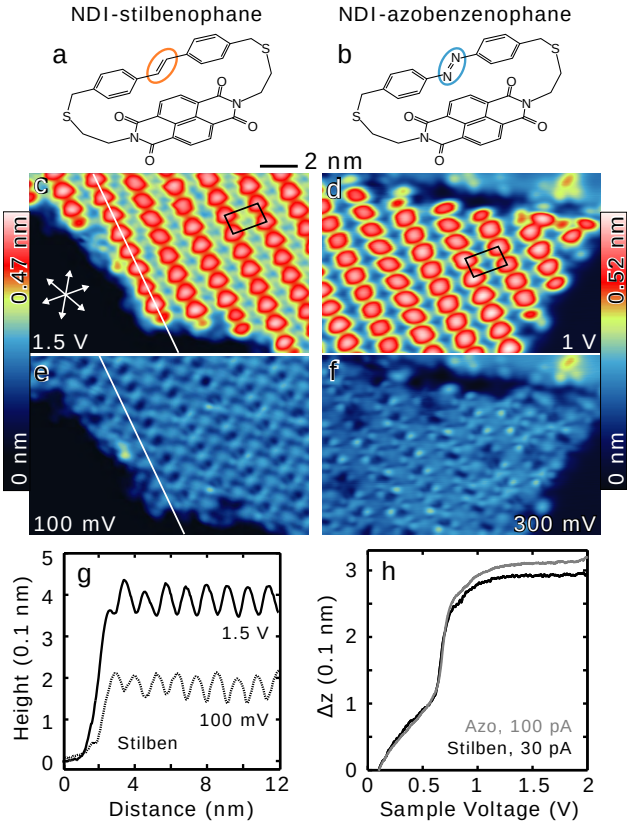

Figure 1: Lewis structures of (a) NDI-stilbenophane and (b) NDI-azobenzenophane. Constant-current topographs of (c, e) NDI-stilbenophane ($I = 70$ pA) and (d, f) NDI-azobenzenophane islands ($I = 20$ pA) on Ag(111) measured at characteristic sample voltages indicated on the images. While the topographs are very similar for NDI-stilbenophane and NDI-azobenzenophane, they vary drastically with the sample voltage. Rectangles mark unit cells. Arrows indicate the compact directions of the substrate, which are identical in all topographs. (g) Cross-sectional profiles along the lines in (c) and (e). (h) Retraction Δz of the tip with sample voltage V at constant-current. Black and gray lines show data from NDI-stilbenophane and NDI-azobenzenophane, respectively, measured above a corner of the unit cells.

STM tip.[34] In our case, the tips are metallic and no change of the tip composition was detected. Moreover, all changes were reversible and exhibited no hysteresis with respect to changes of V. The above facts raise two intriguing questions: (*i*) where are the molecules in these images? And (*ii*) what is the origin of the change of contrast?

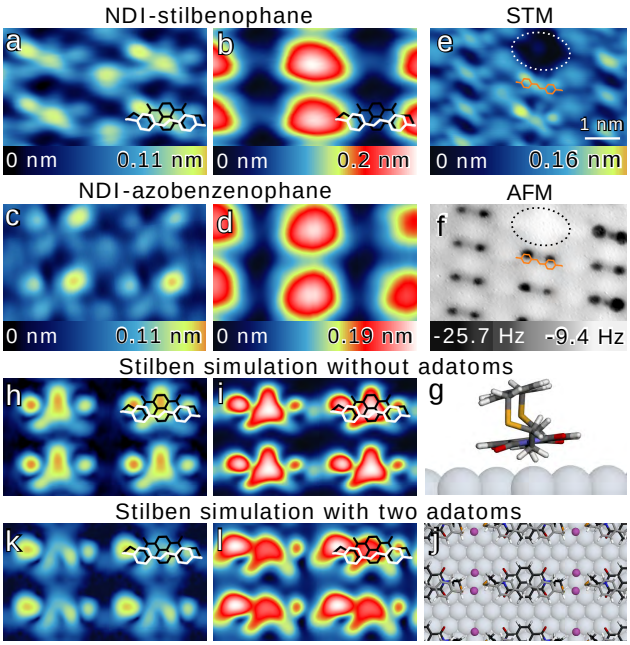

Figure 2: (a, b) Constant-current topographs of a NDI-stilbenophane island recorded at (a) $V = 0.2$ V, $I = 30$ pA and (b) $V = 0.7$ V, $I = 109$ pA. Models of the calculated molecular structure are overlaid. (c, d) Topographs of an NDI-azobenzenophane island measured at (c) $V = 0.2$V, $I = 59$ pA and (d) $V = 0.6$ V, $I = 57$ pA. (e) Topograph of a NDI-stilbenophane island with a defect indicated by a dashed ellipse. $V = 0.1$ V, $I = 30$ pA. (f) AFM frequency shift measured at constant height over the same area as (e) with an oscillation amplitude $A = 0.11$ nm. From the initial tip-sample distance defined by the setpoint $V = 100$ mV and $I = 30$ pA the tip was brought closer to the sample by 80 pm. Phenyl rings, which are the most protruding part of the molecules, cause circular areas of more negative frequency shift. A minor shift is observed from the defect area. (g) Side view of the optimized geometry of NDI-stilbenophane with the NDI platform towards Ag(111). (h, i) Simulated topographs of NDI-stilbenophane at high and low bias without adatoms. (j) Top view of the optimized geometry of NDI-stilbenophane layer intercalated with two adatoms per molecules. (k, l) Like (h) and (i) but with adatoms between adjacent molecules.

To address the first question, Figures 2a–d show the voltage-dependent patterns in more detail. Oval protrusions dominate the topographs at elevated voltage, but are absent at lower voltage in favor of submolecular features. We suggest that the low-bias structures reflect

the position of the molecules whereas the oval observed at higher V is located between the molecules. This counter-intuitive interpretation was initially motivated by the image contrast at occasional defects in the islands. Figure 2e shows a typical example with the defect appearing as a hole (dashed ellipse). This one and all other hole-type defects were found at equivalent positions in the molecular pattern, where they replace topographic maxima of the low-bias pattern.

Non-contact atomic force microscopy (AFM) further corroborates this assignment. Figure 2f shows AFM frequency-shift data measured at constant tip height above the same area as Figure 2e. Pairs of well-defined dots with a negative frequency shift are observed on a submolecular scale. These features occur at the positions of the low-bias maximum in constant current topographs. At the defect (dashed) no significant frequency shift is observed. In addition, the distance between the dots matches the separation of the phenyl rings of stilbene as indicated by the overlaid sketch.

The above observations lead to the conclusion that the low-bias protrusions mark the position of the molecules. Comparison with previous experiments[35,36] of a molecule comprising two identical NDI subunits, shows constant current images distinctly different from the present ones, see Supporting Information. With respect to present cases of NDI-stilbenophane and NDI-azobenzenophane, this additional piece of information shows that the NDI subunit is indeed adsorbed to the substrate rather than facing the STM tip. To confirm this interpretation and to conclude on the origin of the bias-dependent contrast, density functional theory (DFT) calculations were performed (see Methods and Supporting Information),

We obtained the optimized molecular-surface geometry displayed in Figure 2g. The NDI subunit binds to the surface mainly via dispersion interactions with some *dative* contribution from local interactions.[37] Indeed, among the many possibilities to orient the molecule on the surface, an alignment along the high-symmetry direction is preferred due to a minimization of the four O-Ag separations. Figure 2g also shows that the O atoms are slightly bent out

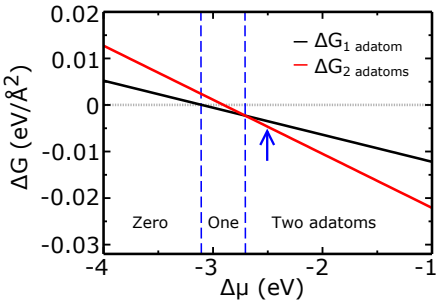

Figure 3: Change in Gibbs free energy ΔG as a function of the change in the Ag chemical potential $\Delta\mu$. Black and red lines correspond to the Gibbs free energy for one and two adatoms co-adsorbed with the molecular layer. Three regions, which are separated by dashed lines, can be discerned in this graph: Zero adatoms are expected where the change in Gibbs free energy becomes positive if adatoms are added, a one-adatom region where the change in free energy minimizes for one adatom, and the two-adatom region where the free energy minimizes for two adatoms. If we assume that the source of adatoms is single adatoms on the clean surface, the equilibrium will be reached close to $\Delta\mu \approx -2.52$ eV (blue arrow) as corresponds to the adsorption energy of single adatoms. However, the chemical potential will shift to lower (absolute value) energies as soon as the source of adatoms are instead edges of steps or islands. Hence, the graph shows that the minimun free-energy at the system's chemical potential corresponds to the two-adatom phase.

of the NDI plane to approach the Ag surface.

This configuration is further validated by comparison with the experimental STM images. We approximate the constant-current images by isocontours of local density of states (LDOS) at finite energies.[30,31] Our simulated images compare well with the experimental ones at low bias (below 0.4 V) when the conformation depicted in Figure 2g is used. However, as the LDOS are plotted at larger bias (*i. e.* energy from the Fermi level) the agreement deteriorates Figure 2i. Moreover, the change in corrugation from the molecules to the interstitial region at ≈ 0.6 V is not reproduced.

Careful examination of the experimental images (Figures 2a–d) shows some structure between the molecules whose apparent height increases as V is ramped up. This may suggest the presence of adatoms between the molecules.

Our total energy calculations predict that adatoms stably coexist with the molecular layer. We performed a thermodynamic study of the Gibbs free energy as a function of the chemical potential of metallic atoms. To that end, we assumed that Ag adatoms can exist on

some part of the surface and that they are in equilibrium with the molecular layer. Hence, the adatoms will enter the molecular layer for chemical potentials comparable to that of the adatom. The Supporting Information contains a detailed account of our thermodynamic calculations. We considered three distinct phases: (*i*) the molecular layer corresponding to no adatoms, (*ii*) the molecular layer with one adatom between the two S atoms of adjacent molecules, (*iii*) a second adatom, close to the previous one (see Figure 2j).

Figure 3 shows the resulting phase diagram. For a large set of chemical potentials around the adatom free energy, the Gibbs free energy of the system is minimal for a phase with two adatoms. In other words, our calculations predict that the phase with two adatoms is the most likely one to be found under the experimental conditions. Adding a third adatom leads to considerable molecular distortion and hence it is not favorable for a large range of chemical potentials. Ag ions are known to form complexes with macrocyclic thio crowns ethers.[38–40] The present case of dialkyl-sulfides appears to be related. On a Ag(111) substrate, the charges of the substrate and a Ag adatom are redistributed to enhance the bonding of the adatom.[41] As a result, the adatom carries a positive charge mimicking a Ag(I) ion. This scenario is different from the adatom-thiol binding on gold surfaces[9,10] where the thiol ending presents a radical S atoms due to the loss of the apical H atom from the molecule.

Our calculations thus lead us to conclude that the studied molecular layer is a hybrid system comprising adatoms and molecules. The driving force for the integration of adatoms is the affinity of the S-terminated edges of the molecule for electrons that enables a directional, *dative*-like bond and the adatom-atom interaction that facilitates the adsorption of the second adatom.

Finally, we address the peculiar voltage-dependent changes of contrast in constant-current STM images. More detailed experimental information is available from spectra of the differential conductance dI/dV, Figures 4a and b for NDI-stilbenophane and NDI-azobenzenophane, respectively. Spectra were recorded on (orange) and between (black) molecules. Overall, the results from both molecules are very similar. The on-molecule spectra repro-

duce the main features of the off-molecule data, namely a sequence of equidistant peaks starting with a sharp rise at 0.5 V. We attribute these features mainly to vibronic excitations.[35] The sharp rise is consistent with the rapid increase of apparent height at this voltage (Figure 1h).

For further analysis, it is important to keep in mind that the area between molecules appears ≈ 0.1 nm higher in constant-current images. On molecules, the tip consequently has to be brought closer by this distance to obtain a comparable conductance. In other words, the amplitudes of all features observed on the molecules are approximately ten times smaller than those between molecules. The fact that the molecular spectrum essentially reproduces the data from interstitial positions may therefore simply reflect the strength and corresponding lateral extent of the latter signal. The only molecular feature that is not observed between the molecules is a small peak at ≈ 0.3 eV.

The experimental observations are only partially reproduced by our calculations. This is largely a consequence of using the LDOS instead of a proper transport calculation to simulate the STM images. A direct comparison of the calculated density of states reproduces some of the observed features, however transport effects, *e.g.* a weak electronic coupling of the upper subunit to the substrate, are not included in the numerical LDOS. According to the calculated projected density of states (PDOS), the LUMO is centered slightly above the Fermi level (Figure 4c, red), in good agreement with the molecular feature observed at 0.3 eV in the dI/dV data. The LUMO is localized to the lower subunit of the molecule, which is consistent with its low conductance. By contrast, the LUMO+1 (blue) is localized to the upper subunit. Its energy matches the dominant spectral features in Figures 4a and b well. By contrast, the p_z states of the adatoms (black), which also extend far into vacuum, are directly coupled to the Ag(111) surface, and become the main conductance channel.

A simulated low-bias STM image of the structure with two Ag adatoms between the S atoms of adjacent molecules is shown in Figure 2k. It reproduces the observed features (Figures 2a and c) quite well. A comparison of the image calculated for elevated bias (Figure 2l)

with the corresponding experimental data (Figures 2b and d) is less favorable. Although features develop in the interstitial region, they are much less dominant than in the experimental images. The contrast in the calculated images is mainly due to the LUMO+1. It is localized to the upper molecular subunit and thus dominates the current in a Tersoff-Hamann description of the tunneling current. The lack of coupling to the substrate, however, is likely to drastically reduce its conductance.

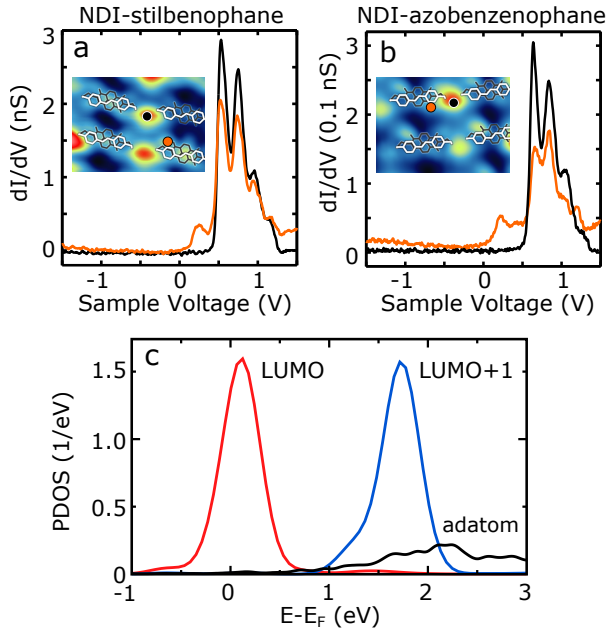

Figure 4: (a) dI/dV spectra of a NDI-stilbenophane molecule. Current feedback was opened at $V = 1.5$ V and $I = 1$ nA. Colored dots in the topograph shown as an inset indicate the positions of measurement. (b) The same type of data as in (a), measured on NDI-azobenzenophane with the feedback opened at $V = 1.5$ V and $I = 0.1$ nA. Above the molecules (orange curves), a rapid rise of dI/dV the onset starts near zero bias in agreement with the calculated energy of the LUMO. At interstial sites (black curves), the rise occurs at lager voltages that match the adatom-induced states displayed in (c). All spectra exhibit a series of approximately equidistant vibronic excitations, which are particularly clear at the interstitial sites. This signal is attributed to the excitation of wagging CH_2 modes. (c) Density of states projected on the indicated molecular orbitals of NDI-stilbenophane (red and blue) and on two adatoms (black).

Conclusions

In summary, adatom dimers are intercalated between NDI-stilbenophane and NDI-azobenzenophanemolecules adsorbed on Ag(111). Two adatoms are compatible with the balance of free energies on the surface, whereas three adatoms are unfavorable. The intermolecular location of these adatoms together with an adatom induced electronic state leads to a fairly sharp onset at 0.5 V in dI/dV spectra. At this voltages the corrugation maximum shifts from ontop of the molecules to an interstitial position. The enhance apparent height of the interstitial area is due to the presence of these intermolecular adatoms and their localized electronic state.

Acknowledgement

KS and RB acknowledge Deutsche Forschungsgemeinschaft for support via SFB 677. MLB thanks the national computational center CINES, and TGCC (Grant 2016- [GENCI project: A0010807364]) for a computer grant. NL greatfully acknowledges support from the MINECO (Grant No. MAT2015-66888-C3-2-R) and FEDER funds. PCH and MM acknowledge financial support by the Swiss National Science Foundation, grant number 200020-159730.

Supporting Information Available

SI-1: Density functional theory calculations. SI-2: Phases with adatoms in the molecular layer. SI-3: Upside-down model compared to symmetric NDI-cyclophane. SI-4: AFM frequency shift of a NDI-azobenzenophane island. SI-5: Orbitals of gas-phase NDI-cyclophane molecules.

References

(1) Vilan, A.; Aswal, D.; Cahen, D. Large-Area, Ensemble Molecular Electronics: Motivation and Challenges. *Chem. Rev.* **2017**, *117*, 4248–4286.

(2) Zrimsek, A. B.; Chiang, N.; Mattei, M.; Zaleski, S.; McAnally, M. O.; Chapman, C. T.; Henry, A.-I.; Schatz, G. C.; Van Duyne, R. P. Single-Molecule Chemistry with Surface- and Tip-Enhanced Raman Spectroscopy. *Chem. Rev.* **2017**, *117*, 7583–7613.

(3) Maurer, R. J.; Ruiz, V. G.; Camarillo-Cisneros, J.; Liu, W.; Ferri, N.; Reuter, K.; Tkatchenko, A. Adsorption Structures and Energetics of Molecules on Metal Surfaces: Bridging Experiment and Theory. *Prog. Surf. Sci.* **2016**, *91*, 72–100.

(4) Böhringer, M.; Berndt, R.; Schneider, W.-D. Transition from Three-Dimensional to Two-Dimensional Faceting of Ag(110) Induced by Cu-Phthalocyanine. *Phys. Rev. B* **1997**, *55*, 1384–1387.

(5) Hinterstein, M.; Torrelles, X.; Felici, R.; Rius, J.; Huang, M.; Fabris, S.; Fuess, H.; Pedio, M. Looking Underneath Fullerenes on Au(110): Formation of Dimples in the Substrate. *Phys. Rev. B* **2008**, *77*, 153412.

(6) Pai, W. W.; Hsu, C.-L. Ordering of an Incommensurate Molecular Layer with Adsorbate-Induced Reconstruction: C_{60}/Ag(100). *Phys. Rev. B* **2003**, *68*, 121403.

(7) Pai, W. W.; Jeng, H. T.; Cheng, C.-M.; Lin, C.-H.; Xiao, X.; Zhao, A.; Zhang, X.; Xu, G.; Shi, X. Q.; Van Hove, M. A. et al. Optimal Electron Doping of a $\mathbf{C}_{60}$ Monolayer on Cu(111) via Interface Reconstruction. *Phys. Rev. Lett.* **2010**, *104*, 036103.

(8) Xie, Y.-C.; Tang, L.; Guo, Q. Cooperative Assembly of Magic Number C60-Au Complexes. *Phys. Rev. Lett.* **2013**, *111*, 186101.

(9) Maksymovych, P.; Voznyy, O.; Dougherty, D. B.; Sorescu, D. C.; Yates Jr., J. T. Gold

Adatom as a Key Structural Component in Self-Assembled Monolayers of Organosulfur Molecules on Au(111). *Prog. Surf. Sci.* **2010**, *85*, 206–240.

(10) Maksymovych, P.; Sorescu, D. C.; Voznyy, O.; Yates, J. T. Hybridization of Phenylthiolate- and Methylthiolate-Adatom Species at Low Coverage on the Au(111) Surface. *J. Am. Chem. Soc.* **2013**, *135*, 4922–4925.

(11) Giovanelli, L.; Savoyant, A.; Abel, M.; Maccherozzi, F.; Ksari, Y.; Koudia, M.; Hayn, R.; Choueikani, F.; Otero, E.; Ohresser, P. et al. Magnetic Coupling and Single-Ion Anisotropy in Surface-Supported Mn-Based Metal-Organic Networks. *J. Phys. Chem. C* **2014**, *118*, 11738–11744.

(12) Lin, N.; Stepanow, S.; Vidal, F.; Barth, J. V.; Kern, K. Manipulating 2D Metal-Organic Networks via Ligand Control. *Chem. Commun.* **2005**, 1681–1683.

(13) Shchyrba, A.; Wäckerlin, C.; Nowakowski, J.; Nowakowska, S.; Björk, J.; Fatayer, S.; Girovsky, J.; Nijs, T.; Martens, S. C.; Kleibert, A. et al. Controlling the Dimensionality of On-Surface Coordination Polymers via Endo- or Exoligation. *J. Am. Chem. Soc.* **2014**, *136*, 9355–9363.

(14) Matena, M.; Stöhr, M.; Riehm, T.; Björk, J.; Martens, S.; Dyer, S., Matthew; Persson, M.; Lobo-Checa, J.; Müller, K.; Enache, M. et al. Aggregation and Contingent Metal/Surface Reactivity of 1,3,8,10-Tetraazaperopyrene (TAPP) on Cu(111). *Chem. Eur. J.* **2010**, *16*, 2079–2091.

(15) Matena, M.; Björk, J.; Wahl, M.; Lee, T.-L.; Zegenhagen, J.; Gade, L. H.; Jung, T. A.; Persson, M.; Stöhr, M. On-Surface Synthesis of a Two-Dimensional Porous Coordination Network: Unraveling Adsorbate Interactions. *Phys. Rev. B* **2014**, *90*, 125408.

(16) Bischoff, F.; He, Y.; Seufert, K.; Stassen, D.; Bonifazi, D.; Barth, J. V.; Auwärter, W. Tailoring Large Pores of Porphyrin Networks on Ag(111) by Metal-Organic Coordination. *Chem. Eur. J.* **2016**, *22*, 15298–15306.

(17) Buchner, F.; Flechtner, K.; Bai, Y.; Zillner, E.; Kellner, I.; Steinrück, H.-P.; Marbach, H.; Gottfried, J. M. Coordination of Iron Atoms by Tetraphenylporphyrin Monolayers and Multilayers on Ag(111) and Formation of Iron-Tetraphenylporphyrin. *J. Phys. Chem. C* **2008**, *112*, 15458–15465.

(18) Umbach, T. R.; Bernien, M.; Hermanns, C. F.; Krüger, A.; Sessi, V.; Fernandez-Torrente, I.; Stoll, P.; Pascual, J. I.; Franke, K. J.; Kuch, W. Ferromagnetic Coupling of Mononuclear Fe Centers in a Self-Assembled Metal-Organic Network on Au(111). *Phys. Rev. Lett.* **2012**, *109*, 267207.

(19) Fan, Q.; Wang, C.; Han, Y.; Zhu, J.; Kuttner, J.; Hilt, G.; Gottfried, J. M. Surface-Assisted Formation, Assembly, and Dynamics of Planar Organometallic Macrocycles and Zigzag Shaped Polymer Chains with CCuC Bonds. *ACS Nano* **2014**, *8*, 709–718.

(20) Wander, A.; Van Hove, M. A.; Somorjai, G. A. Molecule-Induced Displacive Reconstruction in a Substrate Surface: Ethylidyne Adsorbed on Rh(111) Studied by Low-Energy-Electron Diffraction. *Phys. Rev. Lett.* **1991**, *67*, 626–628.

(21) Humblot, V.; Valle, A.; Naitabdi, A.; Tielens, F.; Pradier, C.-M. Drastic Au(111) Surface Reconstruction upon Insulin Growth Factor Tripeptide Adsorption. *J. Am. Chem. Soc.* **2012**, *134*, 6579–6583.

(22) Guaino, P.; Carty, D.; Hughes, G.; McDonald, O.; Cafolla, A. A. Long-Range Order in a Multilayer Organic Film Templated by a Molecular-Induced Surface Reconstruction: Pentacene on Au(110). *Appl. Phys. Lett.* **2004**, *85*, 2777–2779.

(23) Lavrich, D. J.; Wetterer, S. M.; Bernasek, S. L.; Scoles, G. Physisorption and Chemisorption of Alkanethiols and Alkyl Sulfides on Au(111). *J. Phys. Chem. B* **1998**, *102*, 3456–3465.

(24) Sek, S.; Breczko, J.; Plonska-Brzezinska, M. E.; Wilczewska, A. Z.; Echegoyen, L. STM-Based Molecular Junction of Carbon Nano-Onion. *ChemPhysChem* **2012**, *14*, 96–100.

(25) Xu, Y.; Smith, M. D.; Krause, J. A.; Shimizu, L. S. Control of the Intramolecular [2+2] Photocycloaddition in a Bis-Stilbene Macrocycle. *J. Org. Chem.* **2009**, *74*, 4874–4877.

(26) Velema, W. A.; van der Toorn, M.; Szymanski, W.; Feringa, B. L. Design, Synthesis, and Inhibitory Activity of Potent, Photoswitchable Mast Cell Activation Inhibitors. *J. Med. Chem.* **2013**, *56*, 4456–4464.

(27) Kresse, G.; Furthmüller, J. Efficiency of Ab-Initio Total Energy Calculations for Metals and Semiconductors Using a Plane-Wave Basis Set. *Comput. Mater. Sci.* **1996**, *6*, 15–50.

(28) Perdew, J. P.; Burke, K.; Ernzerhof, M. Generalized Gradient Approximation Made Simple. *Phys. Rev. Lett.* **1996**, *77*, 3865.

(29) Tkatchenko, A.; Scheffler, M. Accurate Molecular Van Der Waals Interactions from Ground-State Electron Density and Free-Atom Reference Data. *Phys. Rev. Lett.* **2009**, *102*, 073005.

(30) Tersoff, J.; Hamann, D. R. Theory and Application for the Scanning Tunneling Microscope. *Phys. Rev. Lett.* **1983**, *50*, 1998–2001.

(31) Bocquet, M.-L.; Lesnard, H.; Monturet, S.; Lorente, N. In *Computational Methods in Catalysis and Materials Science*; van Santen, R. A., Sautet, P., Eds.; Wiley-VCH: Weinheim, Germany, 2009; Chapter 11, pp 199–219.

(32) Hess, P. C. NDI-Phanes with Tailor-Made Optical Properties. Ph.D. thesis, Phil.-Nat. Univ. Basel, 2015.

(33) Wesoloski, L. M.; Stieg, A. Z.; Kunitake, M.; Dultz, S. C.; Gimzewski, J. K. Observations of Image Contrast and Dimerization of Decacyclene by Low Temperature Scanning Tunneling Microscopy. *J. Chem. Phys.* **2007**, *127*, 174703.

(34) Calleja, F.; Arnau, A.; Hinarejos, J. J.; Vázquez de Parga, A. L.; Hofer, W. A.; Echenique, P. M.; Miranda, R. Contrast Reversal and Shape Changes of Atomic Adsorbates Measured with Scanning Tunneling Microscopy. *Phys. Rev. Lett.* **2004**, *92*, 206101.

(35) Matino, F.; Schull, G.; Köhler, F.; Gabutti, S.; Mayor, M.; Berndt, R. Electronic Decoupling of a Cyclophane from a Metal Surface. *PNAS* **2011**, *108*, 961–964.

(36) Schneider, N. L.; Matino, F.; Schull, G.; Gabutti, S.; Mayor, M.; Berndt, R. Light Emission from a Double-Decker Molecule on a Metal Surface. *Phys. Rev. B* **2011**, *84*, 153403.

(37) Minkin, V. I. Glosaary of Terms Used in Theoretical Organic Chemistry. *Pure Appl. Chem.* **1999**, *71*, 1919–1981.

(38) Loeb, S. J.; de Groot, B. Encapsulation of Silver(I) by the Crown Thioether Ligand 1,3,6,9,11,14-Hexathiacyclohexadecane (16S6). Synthesis and Structure of [Ag(16S6)][ClO4]. *Inorg. Chem.* **1991**, *30*, 3103–3105.

(39) Blake, A. J.; Gould, R. O.; Holder, A. J.; Hide, T. I.; Schröder, M. Silver Thioether Chemistry: Synthesis, X-Ray Crystal Structure and Redox Properties of [Ag([18]aneS6)]+ ([18]aneS6 = 1,4,7,10,13,16-hexathiacyclooctadecane). *Polyhedron* **1989**, *8*, 513–518.

(40) Alberto, R.; Nef, W.; Smith, A.; Kaden, T. A.; Neuburger, M.; Zehnder, M.; Frey, A.; Abram, U.; Schubiger, P. A. Silver(I) Complexes of the Derivatized Crown Thioether Ligands 3,6,9,12,15,18-Hexathianonadecanol and 3,6,9,13,16,19-Hexathiaicosanol. Determination of Stability Constants and the Crystal Structures of [Ag(19-aneS6-OH)][CF_3SO_3] and [Ag(20-aneS6-OH)][BF_4]. *Inorg. Chem.* **1996**, *35*, 3420–3427.

(41) Limot, L.; Kröger, J.; Berndt, R.; Garcia-Lekue, A.; Hofer, W. A. Atom Transfer and Single-Adatom Contacts. *Phys. Rev. Lett.* **2005**, *94*, 126102.

Graphical TOC Entry